machines

MDPI

Article

Performance Analysis and Hybrid Control Strategy Research of Vehicle Semi-Active Suspension for Ride Comfort and Handling Stability

Fei Wang [1], Hansheng Wen [2] and Sanshan Xie [1,*]

[1] School of Automobile and Transportation, Chengdu Technological University, Chengdu 611730, China; wangfei@cdtu.edu.cn
[2] School of Mechanical Engineering, Beijing Institute of Technology, Beijing 100081, China; 3120245278@bit.edu.cn
* Correspondence: xss730424@cdtu.edu.cn

Abstract: With the advancement of vehicle electrification and intelligence, changes in powertrain system architecture and the addition of battery components have significantly deteriorated vehicle dynamics characteristics. Adjustable damping dampers improve vehicle performance by modifying suspension damping characteristics. Therefore, in this paper, a high-precision multi-dimensional vehicle performance representation model is developed, which includes the dynamics models of the steering and suspension systems and utilizes test results to reflect the constitutive properties of the complex nonlinear structures. The influence regularities of the suspension damping ratio on ride comfort and handling stability are analyzed, and a hybrid control strategy is proposed, which utilizes acceleration-driven damper–Skyhook control logic for vertical control and trigger rule-based control logic for lateral and longitudinal control. Finally, the effectiveness of the control strategy is validated through ride comfort and handling stability tests. The results show that the proposed hybrid control strategy significantly reduces vehicle body vibration acceleration and improves vehicle dynamic response during steering and acceleration/braking conditions.

Keywords: vehicle semi-active suspension; control strategy; ride comfort; handling stability; continuous damping control damper

check for updates

Received: 30 March 2025
Revised: 29 April 2025
Accepted: 2 May 2025
Published: 8 May 2025

Citation: Wang, F.; Wen, H.; Xie, S. Performance Analysis and Hybrid Control Strategy Research of Vehicle Semi-Active Suspension for Ride Comfort and Handling Stability. *Machines* **2025**, *13*, 393. https://doi.org/10.3390/machines13050393

Copyright: © 2025 by the authors. Licensee MDPI, Basel, Switzerland. This article is an open access article distributed under the terms and conditions of the Creative Commons Attribution (CC BY) license (https://creativecommons.org/licenses/by/4.0/).

1. Introduction

The electrification of vehicles has emerged as an inevitable trend in the automotive industry, driven by the global transition in energy infrastructure and growing environmental awareness [1–3]. In recent years, electric vehicles (EVs), with their advantages of high intelligence, low emissions, and superior energy efficiency, have been progressively replacing traditional internal combustion engine vehicles, catalyzing revolutionary advancements in automotive technology [4]. However, the changes in powertrain architecture, modifications to the drivetrain system, and the inclusion of energy storage systems (battery packs) have significantly altered the ratio of sprung to unsprung mass in EVs compared to conventional fuel-powered vehicles. These structural evolutions have led to notable changes in overall vehicle dynamics [5,6]. As a critical interface between the vehicle body and the road surface, the suspension system directly influences both vehicle ride comfort and safety [7,8]. Conventional passive suspension systems, constrained by fixed parameters, struggle to adapt to complex and variable driving conditions, falling short of meeting the modern

demand for integrated vehicle performance [9]. Active suspension systems can expand the dynamic potential of vehicle suspension to a greater extent, which better balances longitudinal and vertical dynamics performance [10]. However, their practical application is constrained by high costs, structural complexity, and excessive energy consumption [11,12]. In contrast, semi-active suspension systems strike an optimal balance between performance enhancement and cost efficiency by adjusting the dynamic characteristics of key actuators, which can quickly respond to road variations without requiring additional energy input. Consequently, they have emerged as a focal point in contemporary research [13]. To realize the broader and faster dynamic adjustment capability of semi-active suspension systems, vehicle component manufacturers have introduced more advanced actuators. However, as the structural design and working mechanisms of these suspension actuators grow increasingly sophisticated, the efficacy of their control strategies becomes pivotal in unlocking their full performance potential. Therefore, in this paper, we focus on the control strategy for the semi-active suspension system to enhance vehicle safety and comfort.

1.1. Related Works on Semi-Active Suspension Control Strategy

The vehicle suspension system comprises stiffness elements, damping elements, and guiding mechanisms [14]. As one of the core components, the damper generates damping forces during relative suspension motion (compression and rebound strokes), which converts mechanical kinetic energy into heat dissipation. This process attenuates vertical body vibrations while maintaining vehicle attitude stability during cornering, rapid acceleration, acceleration, and braking, ensuring optimal tire–road contact and enhancing both handling stability and ride comfort. Continuous damping control (CDC) dampers enable the real-time modulation of damping forces, thereby altering the dynamic characteristics of the suspension system [15]. Kaldas et al. [16] designed an initial pitch control (IPC) for the CDC damper, which is activated during launching, shifting, and braking. The obtained results illustrated that the IPC algorithm with the semi-active controller improved both the pitching motion and road-holding characteristics of the vehicle compared with the passive suspension system. Zhang et al. [17] developed a magnetorheological (MR) semi-active suspension with a half-car decoupled hierarchical optimal sliding mode control strategy. The real-in-loop simulation tests showed that the ride comfort of the semi-active suspension with MR damper was effectively improved. Han et al. [18] proposed a multi-objective intelligent optimization algorithm for MR semi-active suspension to address the vehicle attitude imbalance generated during steering and braking. The simulation results showed that the proposed control method can improve the body roll angle, body pitch angle, and suspension dynamic deflection. Therefore, the dynamic characteristics of adjustable damping dampers have a significant effect on suspension ride comfort and handling stability performance, which should be focused on.

The vehicle system encompasses highly complex dynamic interactions, including multi-dimensional coupling effects in longitudinal, lateral, and vertical directions [19]. Through a high-precision simulation model, the dynamic response process of critical states is calculated to analyze a vehicle's dynamic performance, which can effectively improve the vehicle system's development efficiency and reduce costs. Lai et al. [20] established a unified dynamic mathematical model involving 18 degrees of freedom of a two-axle vehicle based on the coupling relationship of vehicle longitudinal, lateral, and vertical dynamics to evaluate the ride comfort and handling stability of the vehicle. Ataei et al. [21] presented a novel approach in vehicle modeling to provide a unified reconfigurable vehicle dynamics model, which includes two matrices defined as the corner reconfiguration matrix and the actuator reconfiguration matrix. Kou et al. [22] developed the mathematical model of semi-active suspension with a built-in solenoid valve based on AMEsim R16 parametric

simulation software to simulate and analyze dynamic responses and adaptive situations with different sprung masses. Although the establishment of the vehicle dynamics model based on the parametric approach offers simplicity and effectiveness, the equivalence and dimensionality reduction processes often lead to the distortion of complex nonlinear structural constitutive properties. Data-driven approaches, with their superior flexibility, provide an alternative paradigm for vehicle dynamics modeling. Tudon et al. [23] proposed a static model for MR dampers based on artificial neural networks (ANNs) and presented an intensive and experimental study for designing the ANN structure. Chen et al. [24] developed a hybrid model combining physics and dual-attention neural networks to model vehicle lateral dynamics, which can capture spatial and temporal correlations in the vehicle dynamics data. Lee et al. [25] proposed a finite memory estimation algorithm based on neural networks, which is applied to estimate the sideslip angle by combining dynamics and kinematics models. Although data-driven approaches can effectively represent complex nonlinear systems that are difficult to solve by traditional mechanistic modeling approaches, the opaque nature of these black-box models obscures the interpretability of both internal mechanisms and prediction results. Furthermore, model accuracy and generalizability critically depend on the quality and quantity of training data. In contrast, finite element simulation approaches can accurately calculate the complex nonlinear structural constitutive property. To obtain the damping characteristics of the pilot-operated solenoid valve damper, Wen et al. [26] used finite element simulation to calculate the stiffness of the damper disc valve and extracted the deflection characteristics at the throttling port of the disc valve. Hemanth et al. [27] established a semi-active suspension system with an MR damper model and analyzed the magnetic flux density in the fluid flow gap based on the MR field. Mata et al. [28] presented an approach for the formulation of a non-parametric-based polynomial representative model of a magnetorheological damper through coupled computational fluid dynamics and finite element analysis, which was applied to estimate the performance of a quarter car suspension subjected to random road excitation. However, these methods require the establishment of high-quality finite element mesh models, which increases modeling complexity and significantly compromises computational efficiency. Therefore, the challenge is to develop a multi-dimensional vehicle dynamics model, which can accurately and efficiently represent the vehicle dynamic performance.

Vehicle ride comfort [29] refers to the ability of the suspension system to mitigate and dampen vibrations induced by road surface irregularities, while handling stability [30] describes the ability of the suspension system to maintain directional control and resist destabilizing disturbances when subjected to external forces. These performances critically influence both the safety of the vehicle and the physical health of the occupants. To enhance different vehicle dynamic performance, researchers have developed various control strategies for adjustable damping dampers. Zhang et al. [31] proposed a reduced optimization complexity control method to control MR dampers for improving vehicle ride comfort, which combines a dung beetle optimizer, fuzzy control, and proportional–integral–derivative control. Li et al. [32] designed a kind of uncertain structural parameters based on the linear matrix inequality of the H-infinity control strategy. The research showed that a hybrid control strategy can improve the motion reliability and stability of the vehicle. However, these control strategies predominantly focus on improving single-dimensional vehicle dynamic performance. A trade-off exists between ride comfort and handling stability with respect to the damping characteristics of the damper, necessitating integrated design and development. Model predictive control (MPC) methods offer a viable solution for addressing such multi-objective optimization problems, enabling the balanced achievement of multiple control objectives [33]. Kim et al. [34] presented an MPC of a semi-active suspension with a shift delay compensation using preview road information, which was

applied to optimize both ride comfort and road handling performance. Alejandro et al. [35] proposed an autoregressive with exogenous input model-based predictive control strategy to improve passenger comfort and road holding. However, these methods require online optimization problem-solving within each control cycle, resulting in substantial computational complexity and demanding high processing capability from the controller. Consequently, they often fail to meet real-time control requirements. Savaia et al. [36] proposed a novel control strategy derived via a sequential learning framework, which selects the most significant feedback measurements for semi-active control and learns the optimal policy from data. The algorithm is superior in damping the body resonance with respect to the state-of-the-art Skyhook algorithm according to experimental validation. Lee et al. [37] proposed a semi-active suspension ride comfort controller using deep reinforcement learning and designed a state normalization filter to improve the generalization performance. Data-driven control algorithms can achieve control performance beyond the capabilities of conventional strategies while enabling online optimization. However, on the one hand, these methods require extensive vehicle testing to collect training data, which significantly impedes development efficiency; on the other hand, because the performance is entirely dependent on the scenarios and diversity of training data, the reliability and safety need to be further verified, particularly under extreme operating conditions. Therefore, the crucial challenge lies in developing a control strategy which can simultaneously enhance both ride comfort and handling stability.

1.2. Analysis of Related Works

According to the above analysis, many studies have implemented the development of the semi-active suspension control strategy and have achieved effective results; however, the following common problems remain:

(1) In vehicle dynamics modeling, full parametric approaches offer computational efficiency but fail to accurately represent complex nonlinear constitutive properties. For example, the steering system has a steering gap and the damper has a valve open velocity, resulting in strongly nonlinear performance. In addition, experimental testing can directly capture the real performance of critical structures, but they have the problems of high costs and low efficiency. This circumstance leads to a reduction in the effectiveness and efficiency of the control strategy.

(2) In the development of a semi-active suspension control strategy, vehicle performance metrics are multi-dimensional and inherently coupled. Solely optimizing ride comfort degrades handling stability, and an exclusive focus on handling stability compromises occupant comfort. The challenge is to develop a control strategy that simultaneously improves ride comfort and handling stability.

To overcome the aforementioned problems, this paper combines the parametric method and tests and develops a multi-dimensional vehicle performance representation model, which is applied to design a semi-active suspension control strategy to simultaneously improve vehicle ride comfort and handling stability. This paper has two main contributions. (1) A high-precision multi-dimensional vehicle dynamics representation model is developed, which includes the dynamics models of the steering and suspension systems and utilizes test results to reflect the constitutive properties of the complex nonlinear structures. The proposed model can ensure computational efficiency and significantly improve the confidence level. (2) A hybrid control strategy is proposed, which utilizes ADD-SH control logic for vertical control and trigger rule-based control logic for lateral and longitudinal control. The hybrid control strategy simultaneously enhances the vehicle ride comfort and handling stability.

Figure 1 shows the process of vehicle semi-active suspension hybrid control strategy research. Firstly, the nonlinear constitutive property tests of key vehicle systems (steering system and suspension system) are conducted. Then, the multi-dimensional vehicle performance representation model based on test enhancement is established and validated. Subsequently, the ride comfort and handling stability influence regularities are analyzed. Based on the above analysis, the hybrid control strategy is developed, which utilizes the ADD-SH control logic for vertical motion control and trigger rule-based control logic for both lateral and longitudinal motion control. Finally, the control strategy is validated based on the ride comfort and handling stability tests.

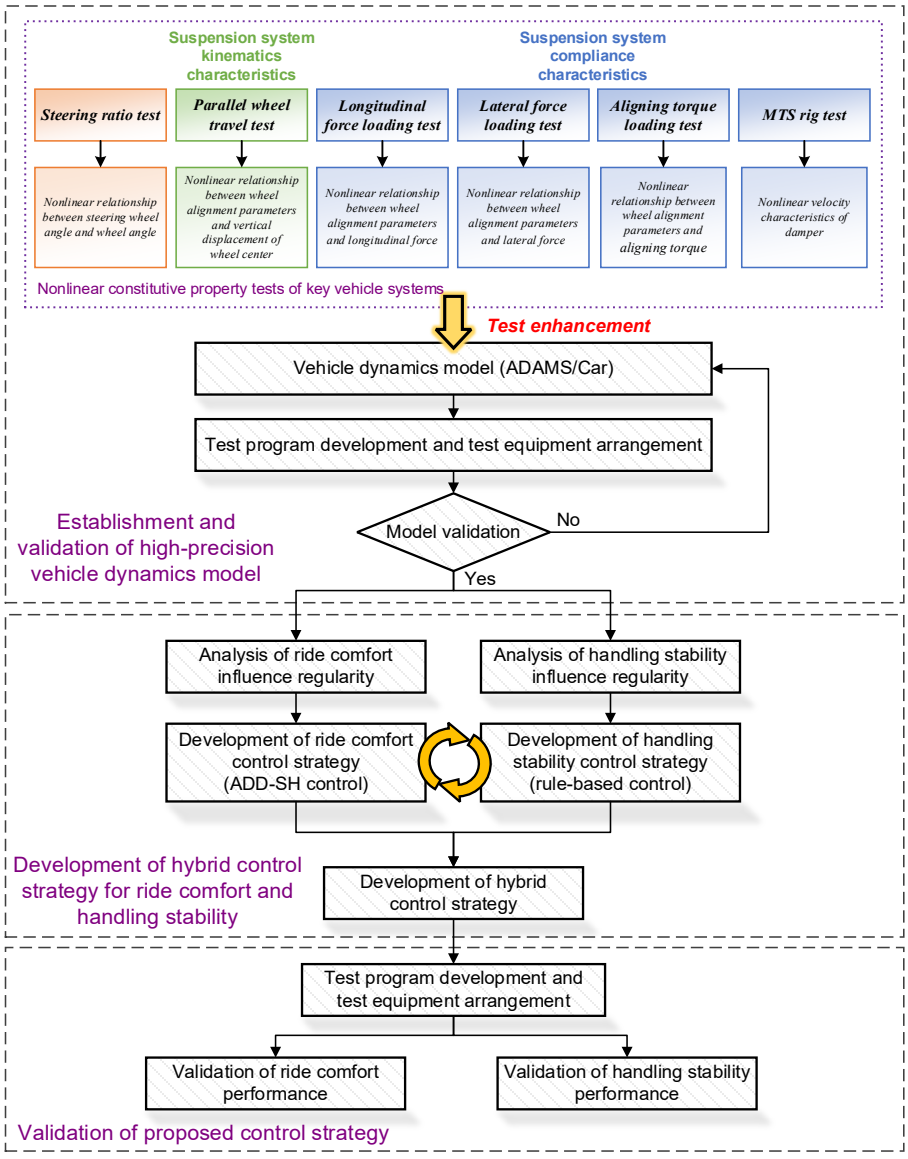

Figure 1. Process of vehicle semi-active suspension hybrid control strategy research.

The remainder of this paper is organized as follows. In Section 2, the high-precision multi-dimensional vehicle performance representation model is established and validated. In Section 3, the influence regularity of suspension damping characteristics on vehicle performance is analyzed and the hybrid control strategy is developed. In Section 4, the control strategy is validated via ride comfort and handling stability tests. Section 5 summarizes the conclusions of this paper.

2. Development of High-Precision Vehicle Dynamics Model

2.1. Establishment of Vehicle Dynamics Model Based on Test Enhancement

2.1.1. Road Model

The frequency-domain power spectral density model for road surface roughness, as standardized by the International Organization for Standardization, is expressed by Equation (1):

$$G_q(n) = G_q(n_0)\left(\frac{n}{n_0}\right)^{-W} \tag{1}$$

where n_0 represents the reference spatial frequency; $G_q(n_0)$ denotes the power spectral density at the reference spatial frequency; and W is the frequency exponent that determines the spectral structure of road surface roughness. The defined power spectral density model in Equation (1) exhibits an overestimation in the low-frequency range compared to the actual road [38]. To address this problem, this paper utilizes a rational function-based expression of the road surface power spectral density [39]:

$$G_q(n) = \frac{\alpha\rho^2}{\pi(\alpha^2 + n^2)} \tag{2}$$

where n denotes the road surface spatial frequency; α represents the road characteristic constant; and ρ corresponds to the road surface roughness variance. The parameter values [40] for α and ρ are given in Table 1.

Table 1. Road models based on rational function.

Road Surface Grades	α (m^{-1})	ρ (mm)
A	0.111	37.7
B	0.111	75.4
C	0.111	150.8
D	0.111	301.6
E	0.111	603.2
F	0.111	1206.4

The time-domain expression of road surface roughness based on Equation (2) is expressed by Equation (3):

$$\dot{q}(t) = -\alpha v q(t) + w(t) \tag{3}$$

where $q(t)$ represents the road surface roughness; v denotes the vehicle speed; and $w(t)$ corresponds to a white noise sequence.

The covariance of the white noise process is expressed by Equation (4):

$$\mathrm{cov}[w(t)] = E[w(t)w(t+\tau)] = 2\rho^2\alpha v\delta(\tau) \tag{4}$$

where τ represents the time lag and $\delta(\cdot)$ denotes the impulse function.

2.1.2. Vehicle Dynamics Model

In this paper, the research object is a passenger car, and the vehicle dynamics equations refer to [41]. The completed subsystem modules are assembled into a vehicle model in Carsim and ADAMS/Car [42]. The subsystem parameters are calibrated to ensure proper data transmission between components. The key vehicle body parameters required for modeling are shown in Table 2.

Table 2. Vehicle parameters.

Parameter	Value
Total mass	1775 (kg)
Front/Rear axle load	1085/690 (kg)
Wheelbase	2750 (mm)
Distance from center of mass to front axle	1050 (mm)
Center of mass height	712 (mm)
Vehicle roll moment of inertia	830 ($kg \cdot m^{-2}$)
Vehicle pitch moment of inertia	3684 ($kg \cdot m^{-2}$)
Vehicle yaw moment of inertia	3420 ($kg \cdot m^{-2}$)
Sprung mass	410 (kg)
Unsprung mass	68.5 (kg)
Vertical stiffness of suspension	31,000 (N/m)
Tire radial stiffness	220,000 (N/m)

To analyze the influence of damper damping characteristics on vehicle ride comfort and handling stability, and then to develop a high-quality semi-active suspension control strategy, a vehicle dynamics simulation model needs to be established. Critically, due to the complex nonlinear constitutive properties of critical system components, tests are used to obtain the nonlinear constitutive relationships of the critical systems (steering system and suspension system) to improve the accuracy of the vehicle dynamics model. The process for high-precision vehicle dynamics modeling based on test enhancement is shown in Figure 2.

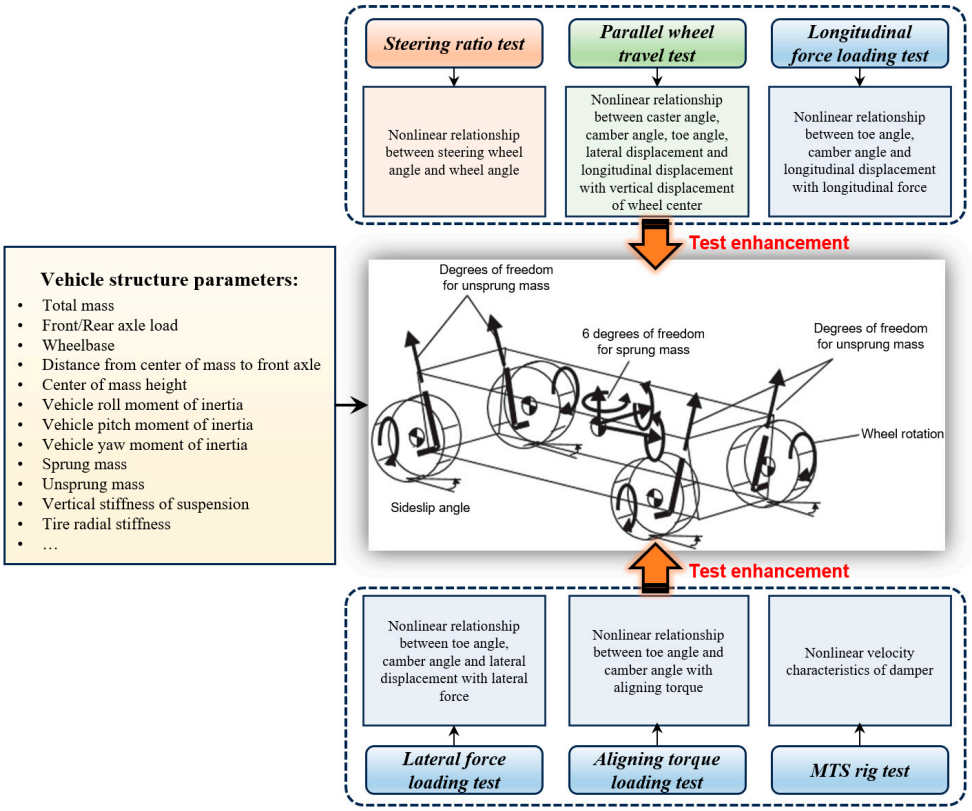

Figure 2. Process for high-precision vehicle dynamics modeling based on test enhancement.

- Steering system dynamics characteristics

The vehicle model established in this paper adopts the rack and pinion steering form. For the steering system modeling, the angle transmission ratio between the steering wheel angle and wheel angle is determined [43]. To enhance model accuracy, a steering ratio

test was performed using an MTS steering test rig, with left-turn rotation defined as the positive direction. The steering ratio test results are shown in Figure 3.

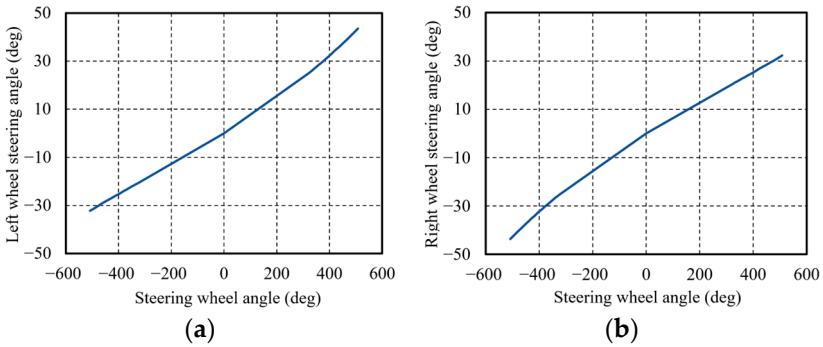

Figure 3. Steering ratio test results. (**a**) Relationship between left front wheel angle and steering wheel angle. (**b**) Relationship between right front wheel angle and steering wheel angle.

- Suspension system kinematics characteristics

Suspension system kinematic characteristics describe the variation in wheel alignment parameters induced by wheel vertical displacement [44]. The suspension system kinematic model involves the relationships between wheel center vertical displacement and caster angle, camber angle, toe angle, wheel lateral displacement, and wheel longitudinal displacement. Figure 4 shows the parallel wheel travel (front and rear suspensions) test results.

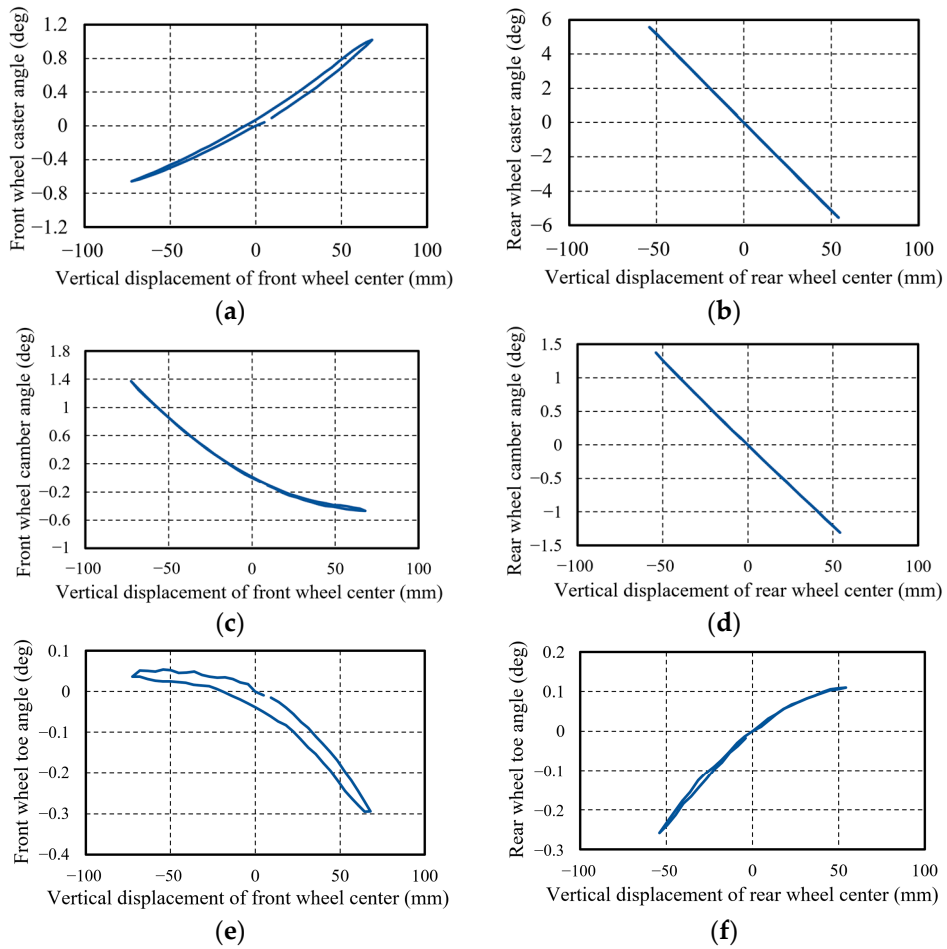

Figure 4. *Cont.*

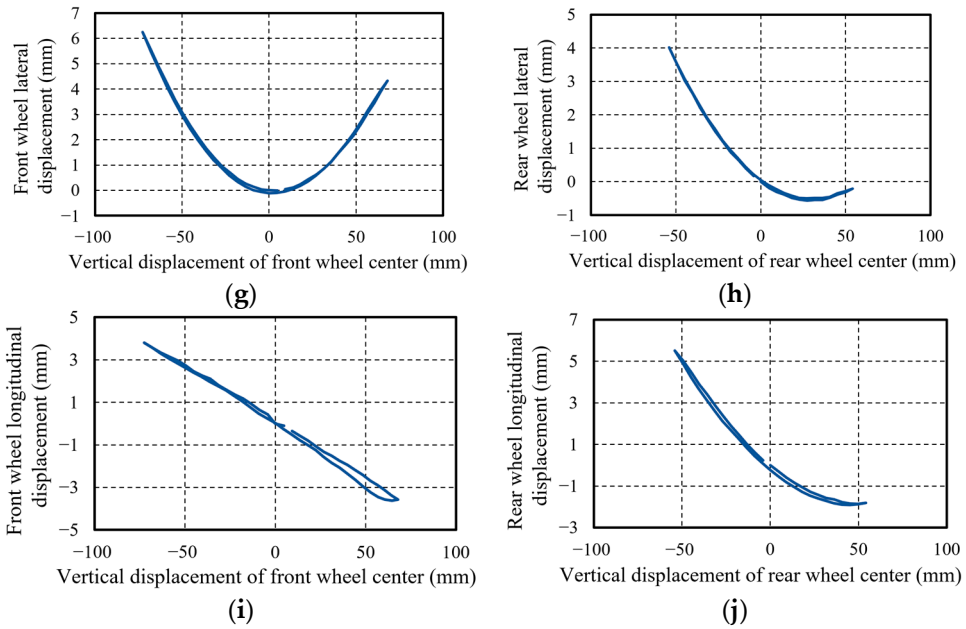

Figure 4. Parallel wheel travel test results. (**a**,**b**) Relationship between caster angle and wheel center vertical displacement. (**c**,**d**) Relationship between camber angle and wheel center vertical displacement. (**e**,**f**) Relationship between toe angle and wheel center vertical displacement. (**g**,**h**) Relationship between wheel lateral displacement and wheel center vertical displacement. (**i**,**j**) Relationship between wheel longitudinal displacement and wheel center vertical displacement.

- Suspension system compliance characteristics

Suspension system compliance characteristics describe the variation in wheel alignment parameters induced by forces and torques at the tire–road interface. The relationships between wheel center longitudinal force and toe angle, camber angle, and wheel longitudinal displacement were obtained from the longitudinal force loading condition test, as shown in Figure 5.

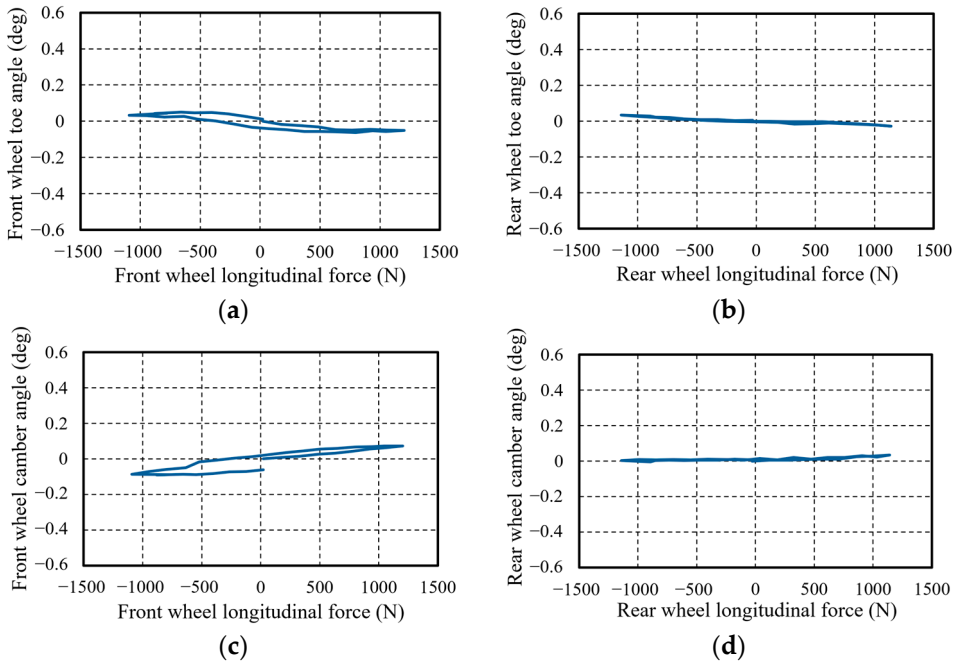

Figure 5. *Cont.*

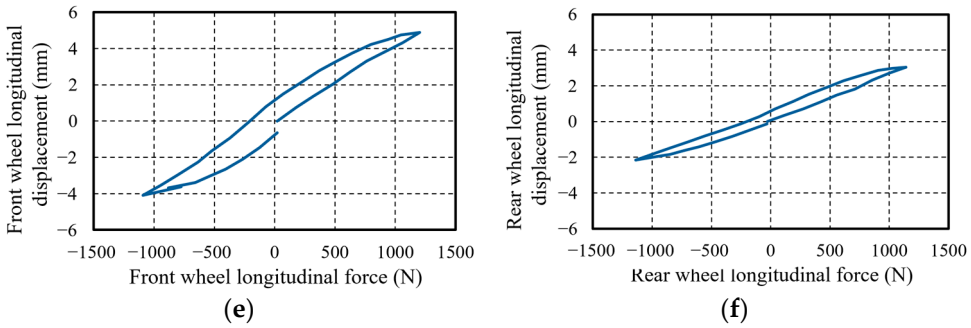

Figure 5. Longitudinal force loading condition test results. (**a**,**b**) Relationship between toe angle and wheel longitudinal force. (**c**,**d**) Relationship between camber angle and wheel longitudinal force. (**e**,**f**) Relationship between wheel longitudinal displacement and wheel longitudinal force.

The relationships between wheel center lateral force and toe angle, camber angle, and wheel lateral displacement were obtained from the lateral force loading condition test, as shown in Figure 6.

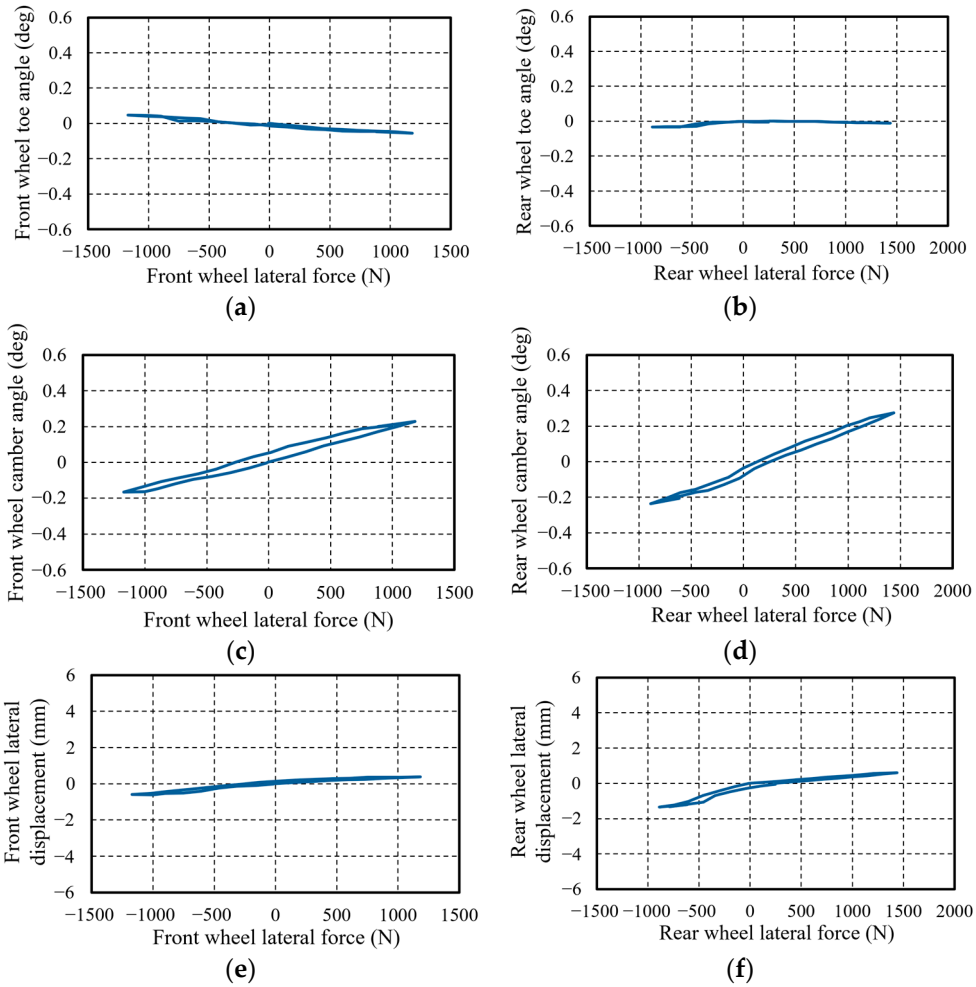

Figure 6. Lateral force loading condition test results. (**a**,**b**) Relationship between toe angle and wheel lateral force. (**c**,**d**) Relationship between camber angle and wheel lateral force. (**e**,**f**) Relationship between wheel lateral displacement and wheel lateral force.

The relationships between wheel center aligning torque and toe angle and camber angle were obtained from the aligning torque loading condition test, as shown in Figure 7.

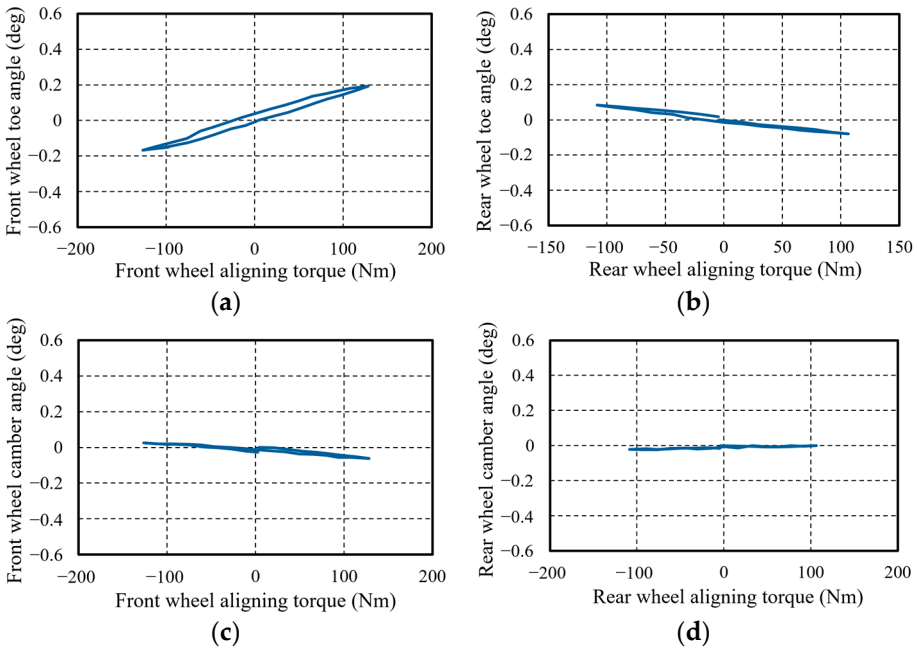

Figure 7. Aligning torque loading condition test results. (**a**,**b**) Relationship between toe angle and wheel aligning torque. (**c**,**d**) Relationship between camber angle and wheel aligning torque.

The velocity characteristics of the damper passive state were measured by the MTS test rig [45]. The test employed fixed displacement amplitude with varying frequency, and the test velocities are 20, 50, 130, 260, 390, 520, and 1,000 mm/s. The damper velocity characteristic curve is shown in Figure 8.

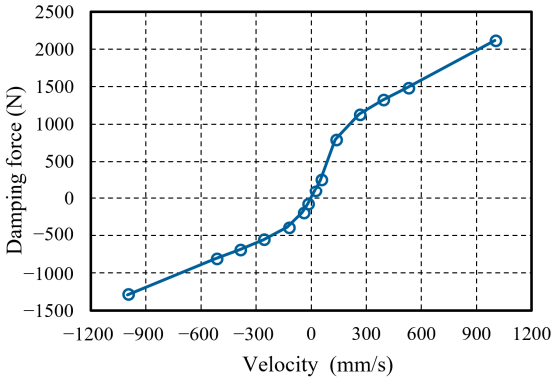

Figure 8. Damper velocity characteristic curve (passive state).

2.2. Vehicle Dynamics Model Validation

To validate the effectiveness of the vehicle dynamics model, the evaluation metrics of ride comfort and handling stability were tested. The tested vehicle parameters are consistent with Table 1. Three vibration acceleration sensors were arranged in the left front, right front, and left rear positions of the vehicle body for the real-time acquisition of body motion signals, and three angle displacement sensors were arranged for the measurement of the rotation angle of the lower arm to realize the real-time acquisition of the relative motion signals of the suspension. The solenoid-controlled CDC damper was applied as the actuator of the semi-active suspension system, and the damper damping characteristics were adjusted by controlling the opening of the solenoid valve, which increases with the increase in the control current. The sensor arrangement schemes and test site are shown in Figure 9.

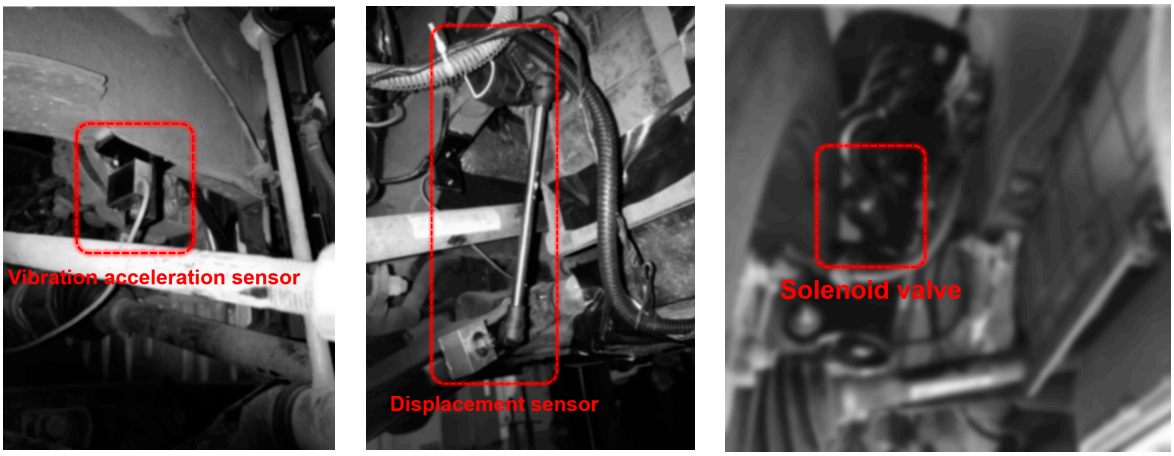

Figure 9. Sensor arrangement schemes and test site. (**a**) Vibration acceleration and displacement sensor mounting positions. (**b**) CDC damper mounting positions.

- Step input of steering wheel angle

According to the standard GB/T 6323-2014 [46], the steering wheel angle step input test was conducted at a vehicle speed of 100 km/h [47]. Within a rise time of 0.2 s, the steering wheel was turned to a preset angle to achieve a steady-state lateral acceleration of 2 m/s^2. During the test, the time course of the yaw rate, roll angle, and lateral acceleration were recorded. The comparisons between the simulation and test curves are shown in Figure 10, while the corresponding parameter results are shown in Table 3. It can be observed that, although some fluctuations exist in the test results, the overall trends of the simulation and test results are consistent, and the steady-state values of all parameters are in good agreement.

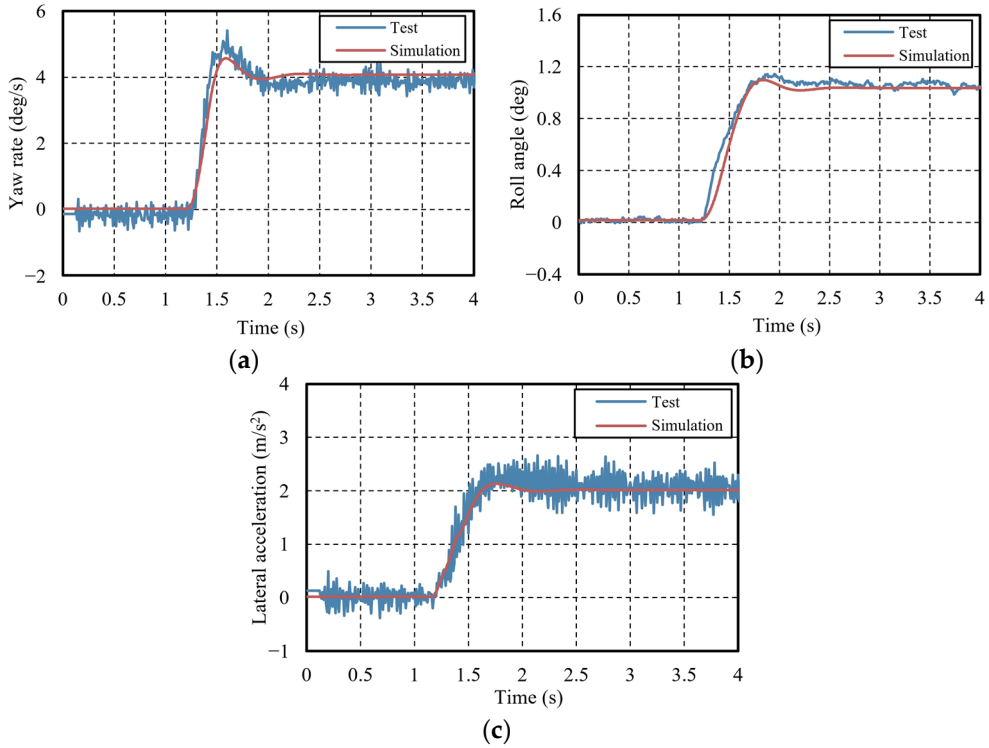

Figure 10. Comparison of simulation and test curves for step input of steering wheel angle. (**a**) Yaw rate. (**b**) Roll angle. (**c**) Lateral acceleration.

Table 3. Comparison of simulation and test results for step input of steering wheel angle.

Angle Step Input Test Metrics	Test Results	Simulation Results	Deviation
Peak value of yaw rate	5.11 deg/s	4.62 deg/s	−9.59%
Steady-state value of yaw rate	4.16 deg/s	4.08 deg/s	−1.92%
Peak value of roll angle	1.14 deg	1.09 deg	−4.39%
Steady-state value of lateral acceleration	2.16 m/s^2	2.02 m/s^2	−6.48%

- Serpentine test

According to the standard GB/T 6323-2014, the serpentine test was conducted at a vehicle speed of 70 km/h [48]. During the test, the time course of the yaw rate, roll angle, and lateral acceleration were recorded. The comparisons between the simulation and test curves are shown in Figure 11, while the corresponding parameter results are shown in Table 4. It can be observed that the simulation results align well with the test results under serpentine conditions.

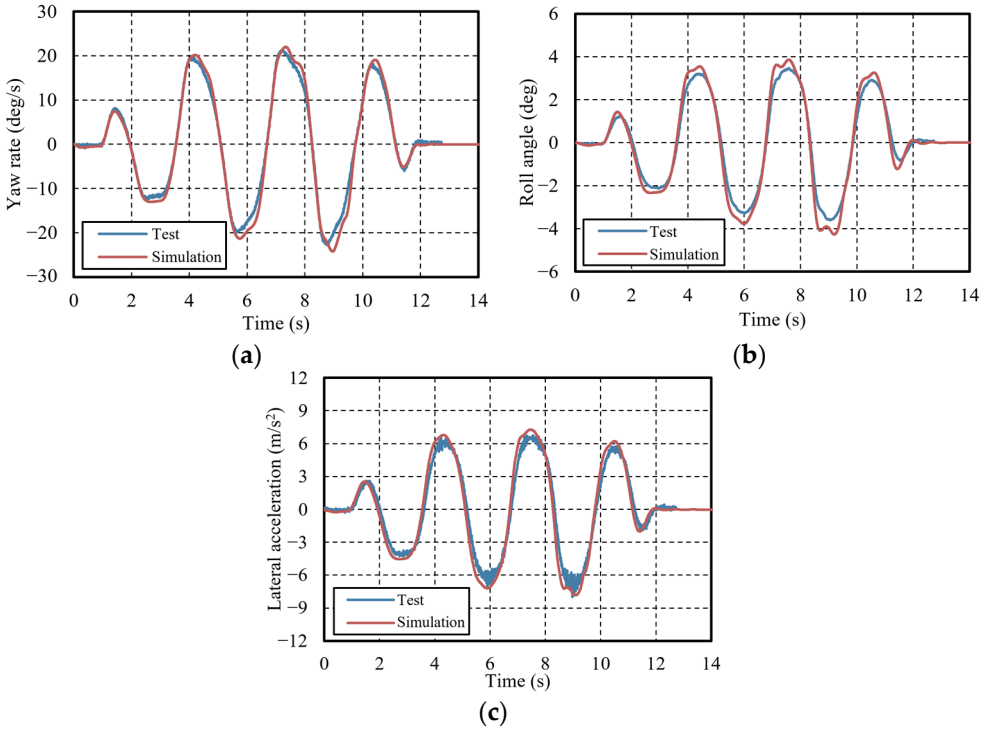

Figure 11. Comparison of simulation and test curves for serpentine test. (**a**) Yaw rate. (**b**) Roll angle. (**c**) Lateral acceleration.

Table 4. Comparison of simulation and test results for serpentine test.

Serpentine Test Metrics	Test Results	Simulation Results	Deviation
Peak average of yaw rate	20.92 deg/s	21.48 deg/s	2.68%
Peak average of roll angle	3.58 deg	3.81 deg	6.42%
Peak average of lateral acceleration	7.12 m/s^2	7.26 m/s^2	1.97%

- Brake test

The braking test was conducted at an initial vehicle speed of 50 km/h, with emergency braking applied until the vehicle completely stopped [49]. During the test, the time course of vehicle speed, pitch angle, and longitudinal acceleration were recorded. The comparisons between the simulation and test curves are shown in Figure 12, while the corresponding

parameter results are shown in Table 5. The results show that the overall trends of the simulation and the test results coincide accurately, which can reflect the transient response characteristics of the vehicle during deceleration.

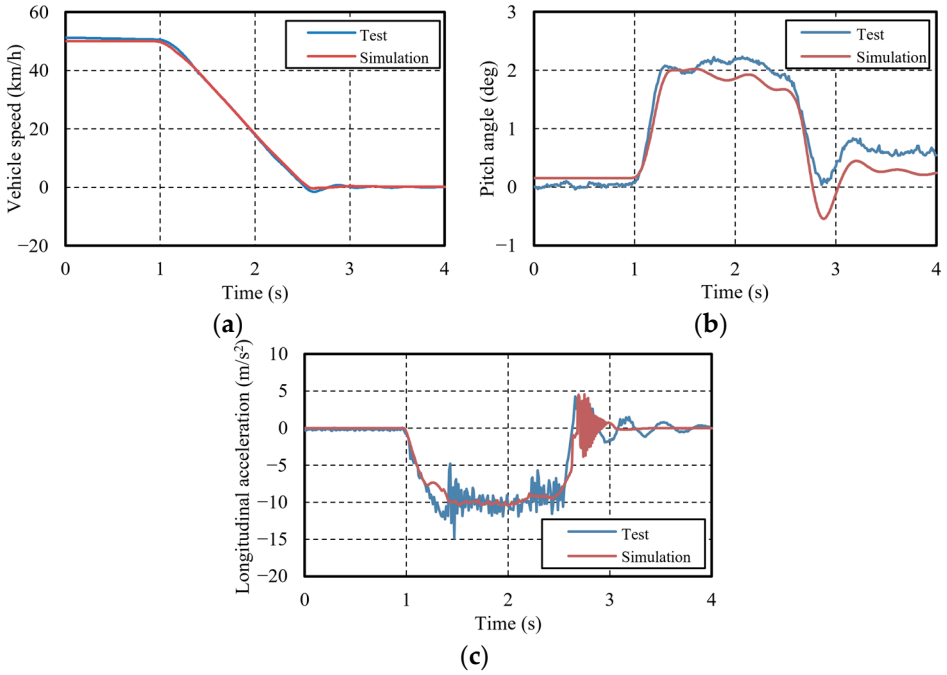

Figure 12. Comparison of simulation and test curves for brake test. (**a**) Vehicle speed. (**b**) Pitch angle. (**c**) Longitudinal acceleration.

Table 5. Comparison of simulation and test results for brake test.

Brake Test Metrics	Test Results	Simulation Results	Deviation
Peak value of pitch angle	2.21 deg	2.02 deg	−8.60%
Peak value of longitudinal acceleration	−10.14 m/s^2	−9.22 m/s^2	−9.07%

In conclusion, the vehicle dynamics simulation model developed in this paper demonstrates a high confidence level and can provide a solid foundation for the analysis of vehicle performance simulation and the development of the control strategy.

3. Development of Hybrid Control Strategy for Ride Comfort and Handling Stability

3.1. Vehicle Performance Influence Regularity Analysis

3.1.1. Ride Comfort Influence Regularity

To investigate the influence of the suspension damping ratio on the ride comfort metrics [50], four typical driving conditions, namely, an A grade road under a vehicle speed of 100 km/h, a B grade road under a vehicle speed of 80 km/h, a C grade road under a vehicle speed of 60 km/h, and a D grade road under a vehicle speed of 40 km/h, were selected [51,52]. The variation trends of body vibration acceleration and wheel dynamic load root mean square (RMS) with the suspension damping ratio are shown in Figure 13. It can be observed that optimal damping ratios ξ_c and ξ_s exist for minimizing the RMS values of both vehicle body acceleration and wheel dynamic load across all conditions. In addition, ξ_c and ξ_s remain independent of both road surface grade and vehicle speed. Within the optimal damping ratio range (ξ_c to ξ_s), the following trends are observed: (1) the body acceleration RMS consistently increases with increasing damping

ratio; (2) the wheel dynamic load RMS consistently decreases with increasing damping ratio; and (3) the sensitivity of the RMS values of both vehicle body acceleration and wheel dynamic load to damping ratio variations becomes progressively more pronounced as road conditions deteriorate. These findings indicate that ride comfort and driving safety need to be harmonized and compromised in this range.

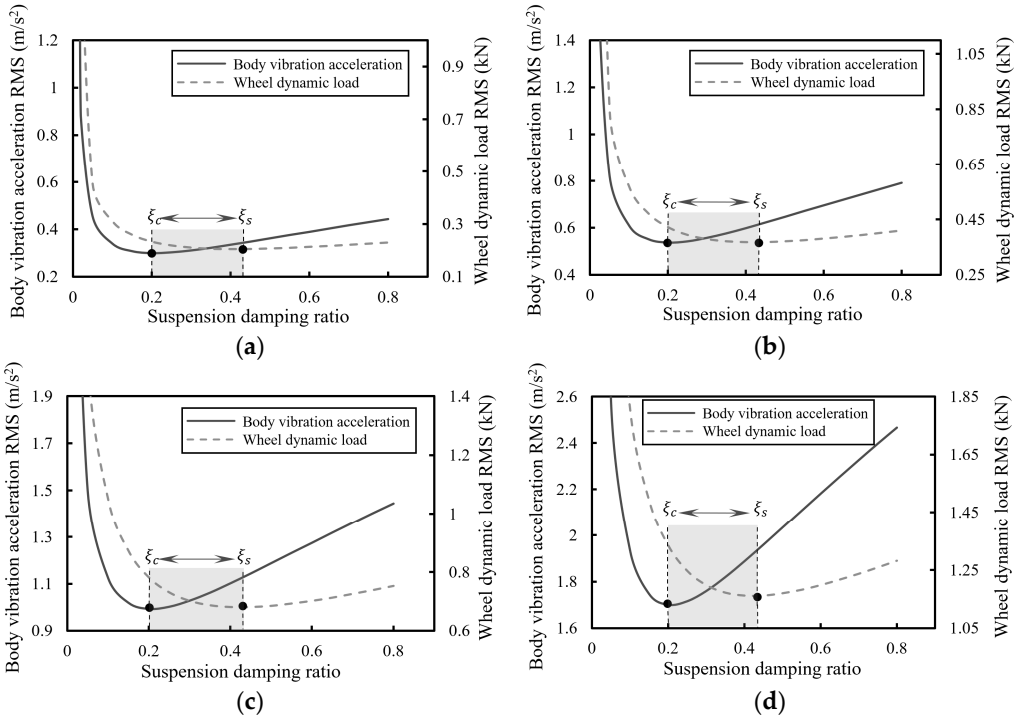

Figure 13. The variation trends of body vibration acceleration and wheel dynamic load RMS with the suspension damping ratio. (**a**) A grade road under a vehicle speed of 100 km/h. (**b**) B grade road under a vehicle speed of 80 km/h. (**c**) C grade road under a vehicle speed of 60 km/h. (**d**) D grade road under a vehicle speed of 40 km/h.

3.1.2. Handling Stability Influence Regularity

Under a vehicle speed of 100 km/h and a steady-state lateral acceleration of 2 m/s^2, the time course response curves of suspension performance for the step input of the steering wheel angle are shown in Figure 14. Figure 14a shows that variations in damping characteristics influence both the peak response and fluctuation amplitude of the roll angle, where the peak roll angle directly correlates with roll overshoot, which describes transient roll response characteristics. Figure 14b shows that damping characteristics influence the roll response rate, with the driver showing greater sensitivity to roll rate variations than the roll angle. Minimizing the peak roll rate substantially improves driver confidence during the steering process. In summary, increasing damping during steering maneuvers can delay roll dynamic response, suppress excessive transient roll overshoot, and improve both roll stability and driver confidence.

Figure 14c,d show that the variations in damping characteristics will affect the response peak and fluctuation amplitude of the yaw rate and lateral acceleration. It can be seen that increasing damping during steering maneuvers can improve the transient response characteristics of the yaw and lateral direction, so that the yaw rate and lateral acceleration tend to stabilize faster.

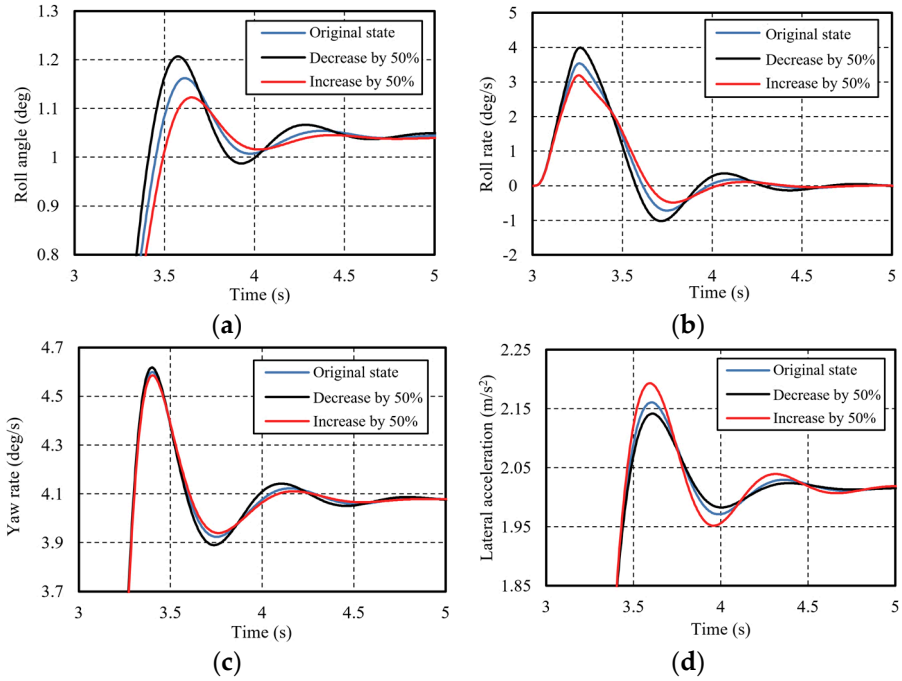

Figure 14. Time course response curves of suspension performance for step input of steering wheel angle. (**a**) Roll angle. (**b**) Roll rate. (**c**) Yaw rate. (**d**) Lateral acceleration.

Under a vehicle speed of 70 km/h, the time course response curves of suspension performance for the serpentine test are shown in Figure 15. It can be seen that variations in damping characteristics affect the peak values of both roll angle and roll rate, with a more noticeable influence on the peak roll rate. These findings demonstrate that increasing damping during continuous steering can improve the roll resistance to a certain degree.

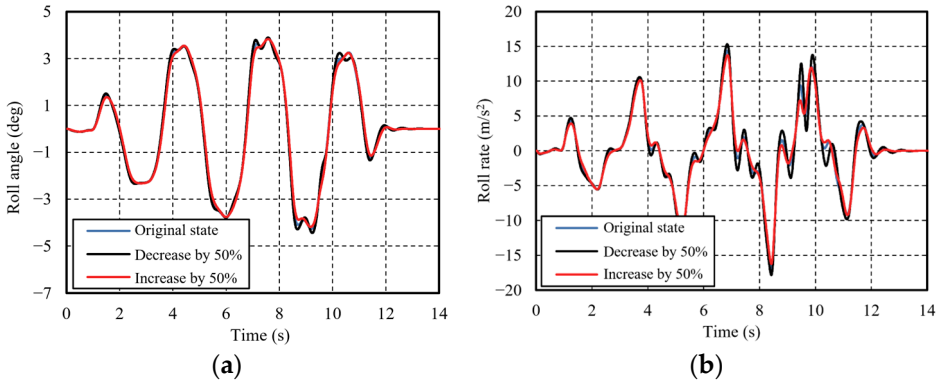

Figure 15. Time course response curves of suspension performance for serpentine test. (**a**) Roll angle. (**b**) Roll rate.

With an initial vehicle speed of 50 km/h, the time course response curves of suspension performance for the brake test are shown in Figure 16. The variation trends of the curves reveal that variations in damping characteristics significantly affect both the peak response and oscillation amplitude of the vehicle pitch angle, as well as the pitch response rate. These results demonstrate that increasing damping during braking can effectively suppress body pitch motion and improve the transient response characteristics in the longitudinal direction.

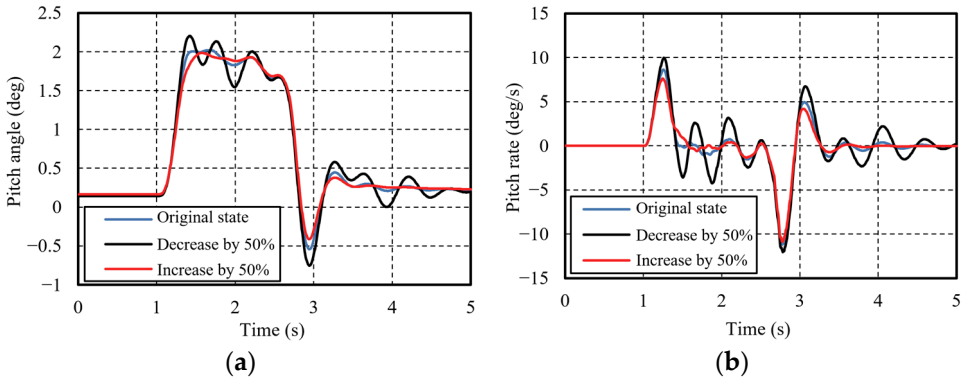

Figure 16. Time course response curves of suspension performance for brake test. (**a**) Pitch angle. (**b**) Pitch rate.

Based on the simulation results of the three typical test conditions described above, it can be concluded that increasing suspension damping can effectively improve the transient response characteristics of both lateral and longitudinal motions. This enhancement reduces load transfer caused by roll or pitch during dynamic responses, thereby improving the handling and stability performance of the vehicle in both lateral and longitudinal directions. These findings demonstrate that semi-active suspension systems can improve vehicle handling stability by continuously monitoring driver inputs and vehicle motion states, while utilizing control systems to adjust suspension damping characteristics in a timely and appropriate manner.

3.2. Hybrid Control Strategy Development

3.2.1. Ride Comfort Control Strategy

By combining the performance advantages of both Skyhook (SH) control and acceleration-driven damper (ADD) control [53], the composite ADD-SH control strategy can effectively suppress vehicle body vibrations across the full frequency range of road excitations. The control logic is expressed by Equation (5):

$$c_s = \begin{cases} c_{max}, \ if \quad \left[\left(\ddot{x}_s{}^2 - \alpha_f{}^2 \dot{x}_s{}^2\right) \le 0 \ and \ \dot{x}_s \dot{x}_{su} > 0\right] \\ \qquad\qquad OR\left[\left(\ddot{x}_s{}^2 - \alpha_f{}^2 \dot{x}_s{}^2\right) > 0 \ and \ \ddot{x}_s \dot{x}_{su} > 0\right] \\ c_{min}, \qquad\qquad\qquad\qquad\qquad\qquad otherwise \end{cases} \tag{5}$$

where c_s is the damping coefficient of the CDC damper; c_{min} and c_{max} are the minimum and maximum damping coefficients of the CDC damper, respectively; x_s and x_{su} are the vehicle body motion velocity and the suspension relative motion velocity, respectively; and α_f is the tuning parameter of the ADD-SH control logic. According to the invariant point characteristic of the suspension, $\alpha_f = \sqrt{k_s/2m_s\pi^2}$.

3.2.2. Handling Stability Control Strategy

Section 3.1 demonstrates that increasing damping during steering maneuvers can effectively reduce the roll rate while improving steering response characteristics. To achieve effective lateral motion control, it is essential to clarify the vehicle state information and the triggering conditions for control activation. Based on the simulation results of the steering wheel angle step test under the original damping state presented in Section 3.1, the normalized results are shown in Figure 17. The results demonstrate that when the steering wheel angle is input, the lateral acceleration responds immediately, followed by the yaw rate, which exhibits faster response dynamics than lateral acceleration. When lateral acceleration reaches a certain threshold, the vehicle roll angle begins to respond

with characteristic followability to the lateral acceleration. After steering input completion, all response parameters require a finite duration to stabilize at new steady-state values. Therefore, the steering wheel angle velocity can be employed as the state parameter for identifying driver steering behavior and intention anticipation, while the lateral acceleration serves as the state parameter for evaluating vehicle roll severity. These two parameters should be synergistically utilized as triggering criteria for lateral motion control, ensuring that the control system can execute timely and effective interventions during both the initial steering input stage and the subsequent lateral dynamic response process.

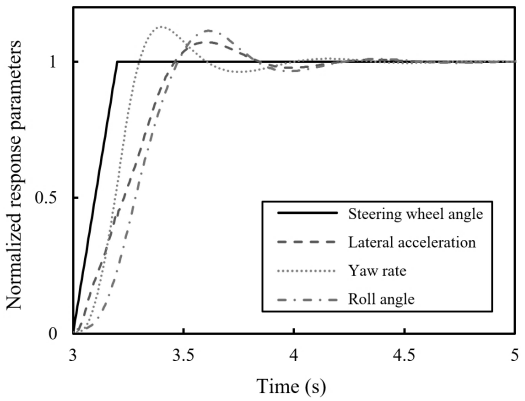

Figure 17. Normalized response parameters for step input of steering wheel angle.

Based on the above analysis, the lateral motion control logic is formulated as follows: the steering wheel angle velocity $\dot{\delta}$ and lateral acceleration a_y are applied as the state parameters for lateral control. When $\dot{\delta}$ reaches the steering wheel angle velocity threshold $\dot{\delta}_{ref}$ or a_y reaches the lateral acceleration threshold a_{y-ref}, the lateral control is triggered, and the control system adjusts the damping coefficient to c_y to suppress the vehicle body yaw and roll motions. When $\dot{\delta}$ is less than $\dot{\delta}_{ref}$ and a_y is less than a_{y-ref}, the lateral control is exited. The control logic is expressed in Equation (6):

$$c_s = c_y, \ \ if \ \left|\dot{\delta}\right| \geq \dot{\delta}_{ref} \ OR \ \left|a_y\right| \geq a_{y-ref} \tag{6}$$

Similarly, when the driver applies acceleration or braking, increasing damping can effectively suppress the peak pitch angle and the pitch rate. Analogously to lateral control, the longitudinal control logic is formulated as follows: the acceleration (brake) pedal rate $\dot{\beta}_a$ ($\dot{\beta}_b$) and longitudinal acceleration a_x are applied as the state parameters for longitudinal control. When $\dot{\beta}_a$ ($\dot{\beta}_b$) reaches the longitudinal acceleration threshold $\dot{\beta}_{a-ref}$ ($\dot{\beta}_{b-ref}$) or a_x reaches the longitudinal acceleration threshold a_{x-ref}, the longitudinal control is triggered, and the control system adjusts the damping coefficient to c_x to suppress the vehicle body pitch motion. When $\dot{\beta}_a$ ($\dot{\beta}_b$) is less than $\dot{\beta}_{a-ref}$ ($\dot{\beta}_{b-ref}$) and a_x is less than a_{x-ref}, the longitudinal control is exited. The lateral control parameter c_y and the longitudinal control parameter c_x are calibrated by vehicle tests. The control logic is expressed in Equation (7):

$$c_s = c_x, \quad if \ \ \dot{\beta}_a \geq \dot{\beta}_{a-ref} \ OR \ \dot{\beta}_b \geq \dot{\beta}_{b-ref} \ OR \ |a_x| \geq a_{x-ref} \tag{7}$$

3.2.3. Hybrid Control Strategy

Based on the above analysis, the hybrid control strategy utilizes the ADD-SH control logic for vertical motion control and trigger rule-based control logic for both lateral and longitudinal motion control. To ensure effective implementation in semi-active suspension systems for the comprehensive improvement of ride comfort and handling stability, the switching rules between these control logics must be established.

When the above control logics operate simultaneously, the damping output Y_c of the ride comfort control strategy and the damping output Y_s of the handling stability control strategy need to be arbitrated. Among them, the damping output Y_c adopts the above ADD-SH control scheme, and the control logic is expressed in Equation (8):

$$Y_c = \begin{cases} c_{max}, \ if \quad \left[\left(\ddot{x}_s{}^2 - \alpha_f{}^2 \dot{x}_s{}^2\right) \le 0 \ and \ \dot{x}_s \dot{x}_{su} > 0\right] \\ \qquad OR \left[\left(\ddot{x}_s{}^2 - \alpha_f{}^2 \dot{x}_s{}^2\right) > 0 \ and \ \ddot{x}_s \dot{x}_{su} > 0\right] \\ c_{min}, \qquad\qquad otherwise \end{cases} \tag{8}$$

The control logic should ensure that the handling stability damping output Y_s prioritizes higher damping values when either lateral or longitudinal control is triggered. The control logic is expressed in Equation (9):

$$Y_s = \begin{cases} max(c_x, c_y), & if \ A \\ 0, & otherwise \end{cases} \tag{9}$$

where A is $\left|\dot{\delta}\right| \ge \dot{\delta}_{ref} \ OR \ |a_y| \ge a_{y-ref} \ OR \ \dot{\beta}_a \ge \dot{\beta}_{a-ref} \ OR \ \dot{\beta}_b \ge \dot{\beta}_{b-ref} \ OR \ |a_x| \ge a_{x-ref}$.

4. Test Validation of Proposed Control Strategy

4.1. Ride Comfort Performance Validation

To validate the improvement effect of the proposed control strategy on vehicle ride comfort, vibration acceleration responses were collected through vehicle ride comfort tests. The tested vehicle is consistent with Section 2.2. The tests were conducted at an automotive proving ground by the standard GB/T 4970-2009 [54] and ISO 2631-1:1997 [55]. The Belgian road [56], a typical characteristic pavement for ride comfort evaluation, was selected as the test condition, with vehicle speeds set at 40 km/h and 60 km/h. Since the human body is most sensitive to vertical vibrations, the vertical vibration acceleration RMS value between 0 and 100 Hz frequency band was applied as the ride comfort objective metric [57]. Acceleration vibration sensors were arranged on the seat and floor of both the driver and the rear passenger on the same side to collect vibration signals. Signal acquisition was performed using a 24-channel LMS Test.Lab front-end system, configured with a frequency resolution of 5120 Hz, a sampling frequency of 1 Hz, and a sampling time of 1 s. The test site is shown in Figure 18.

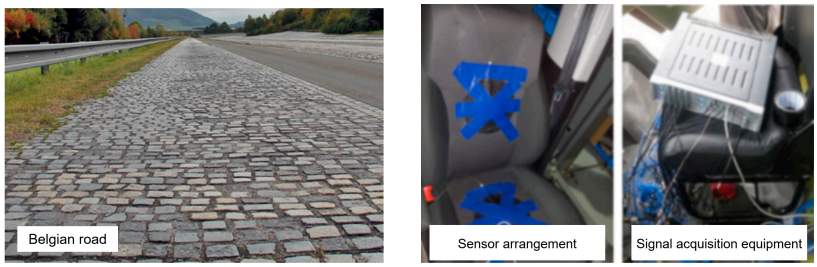

Figure 18. Sensor arrangement positions, signal acquisition equipment, and test site.

The suspension system was tested in the passive state (the CDC damper in the uncontrolled state) and the semi-active state (the CDC damper controlled by the developed strategy). The comparison curves of the vibration acceleration signals collected at different vehicle speeds and in the two states after spectral processing are shown in Figures 19 and 20, and the RMS values are calculated as shown in Table 6. It can be seen that with the increase in the vehicle speed, the power spectral density of vibration acceleration at each position increases, and the vibration acceleration at the driver (passenger) seat is higher than that at

the floor. In comparison, the RMS values in the concerned frequency band are lower than the passive state of the suspension system when adjusted by the CDC damper according to the developed control strategy. However, the vibration acceleration amplitudes at the driver seat increase at some frequency points under the developed control strategy, which is because the vibration acceleration results at the measurement points are affected by the characteristics of the seat cushion sponge. But that does not affect the overall control effect. The results demonstrate that the developed control strategy achieves excellent vibration isolation performance and greatly improves vehicle ride comfort.

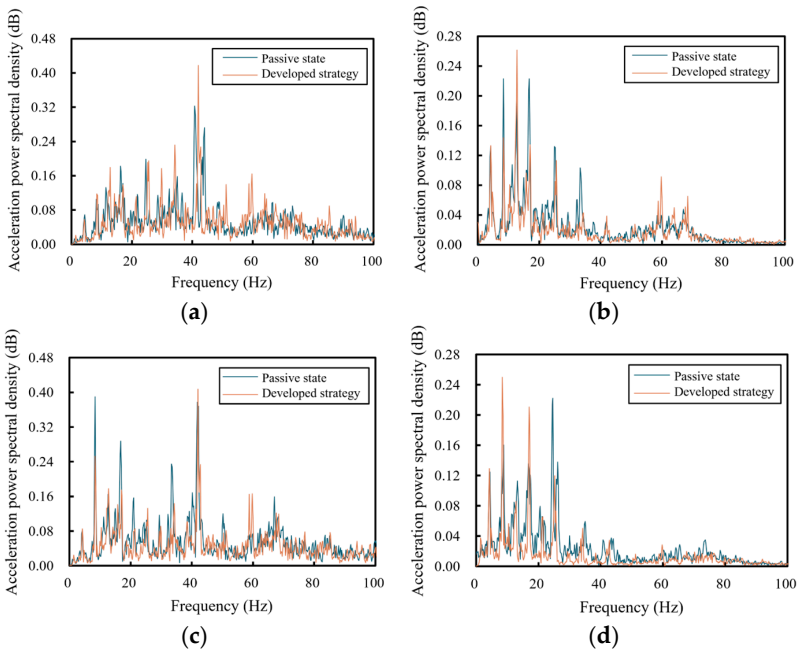

Figure 19. Comparison of vibration acceleration frequency domain curves at 40 km/h. (**a**) Driver floor vertical direction. (**b**) Driver seat vertical direction. (**c**) Passenger floor vertical direction. (**d**) Passenger seat vertical direction.

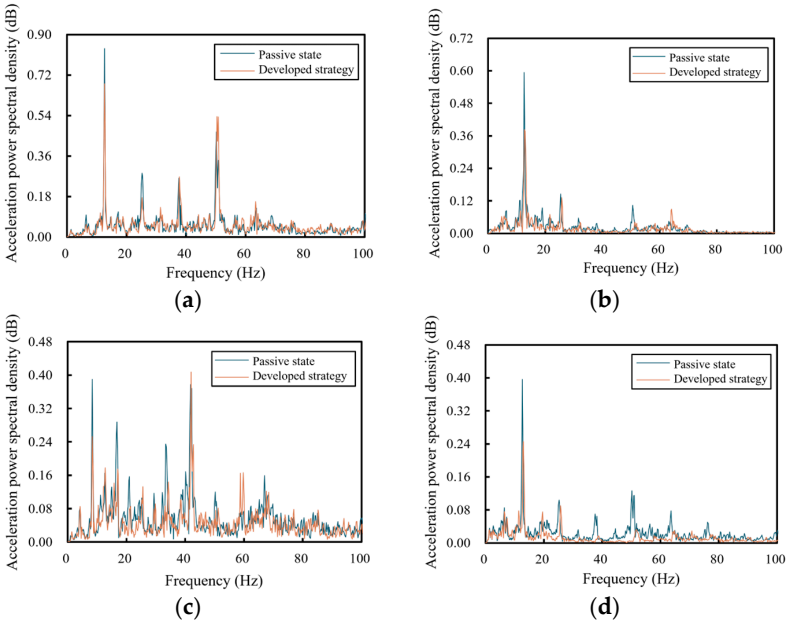

Figure 20. Comparison of vibration acceleration frequency domain curves at 60 km/h. (**a**) Driver floor vertical direction. (**b**) Driver seat vertical direction. (**c**) Passenger floor vertical direction. (**d**) Passenger seat vertical direction.

Table 6. Comparison of vibration acceleration RMS of ride comfort objective test.

Working Condition	RMS Value of Vertical Vibration Acceleration (m/s^2)							
	Driver Seat		Driver Floor		Passenger Seat		Passenger Floor	
	Passive State	Developed Strategy	Passive State	Developed Strategy	Passive State	Developed Strategy	Passive State	Developed Strategy
40 km/h	1.21	1.18	0.69	0.60	1.34	1.09	0.68	0.51
60 km/h	1.54	1.50	0.83	0.70	1.43	1.32	0.66	0.45

4.2. Handling Stability Performance Validation

To validate the improvement effect of the developed control strategy on vehicle handling stability, the time course response curves of suspension performance were collected through the double lane change test and acceleration and braking tests [58]. The tested vehicle is consistent with Section 2.2. According to the ISO 3888-1:2018 standard [59], the double lane change test was conducted to evaluate the vehicle lateral motion response characteristics under continuous steering wheel large angle inputs. At a speed of 30 km/h, the steering wheel angle was set as the input, and the time course response curves of the roll angle and roll rate were collected, as shown in Figure 21. The results demonstrate that the proposed control strategy significantly improves the vehicle roll angle and roll rate responses compared to the suspension passive state.

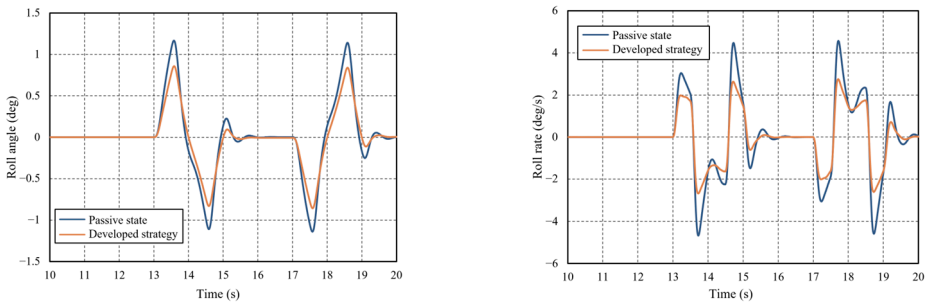

(**a**) (**b**)

Figure 21. Time course response curves of suspension performance for double lane change test. (**a**) Roll angle. (**b**) Roll rate.

In addition, the longitudinal motion response characteristics under larger longitudinal acceleration input are reflected in the acceleration and braking tests. With the prescribed target vehicle speed input, the time course response curve of the pitch rate was collected as shown in Figure 22. Similarly, the pitch rate in the acceleration and braking processes are lower in the suspension semi-active state than in the passive state. The results demonstrate that the developed control strategy provides excellent body attitude control performance and greatly improves vehicle handling stability.

In addition, a subjective evaluation was conducted in parallel with the objective tests [60]. The comparison of the subjective evaluation scores for the suspension passive and semi-active states is shown in Figure 23. Compared with the passive state, the scores of the subjective evaluation metrics in the semi-active state are significantly improved, and the improvement in road feel is especially obvious.

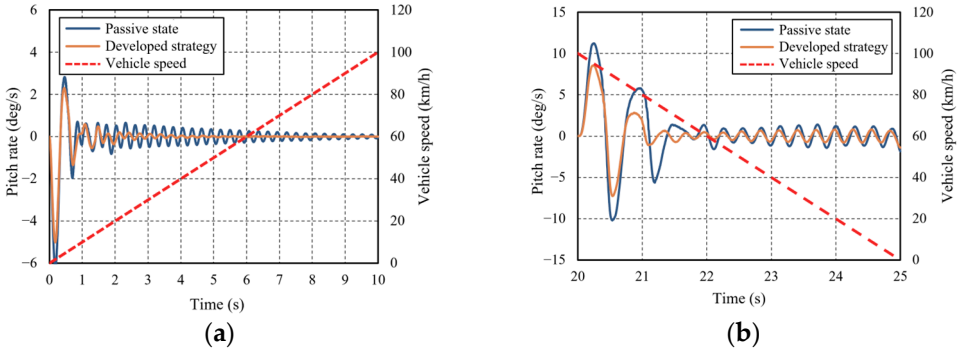

Figure 22. Time course response curve of pitch rate for acceleration and braking tests. (**a**) Acceleration process. (**b**) Braking process.

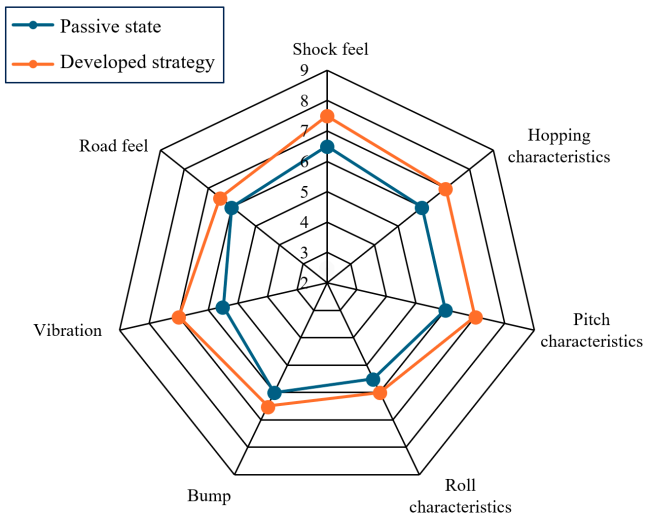

Figure 23. Comparison of subjective evaluation scores.

Combining the above subjective and objective test results of the ride comfort and handling stability, it can be concluded that the semi-active suspension hybrid control strategy developed in this paper improves the vehicle ride comfort, but also enhances the vehicle handling stability and safety, achieving excellent control performance.

5. Conclusions

In this paper, we combined the parametric method and tests and developed a multi-dimensional vehicle performance representation model, which was applied to design a semi-active suspension control strategy to improve vehicle ride comfort and handling stability. The constitutive properties of the complex nonlinear structures (steering system dynamics characteristics, suspension system kinematics, and compliance characteristics) were obtained to achieve test enhancement for the vehicle parametric model. The vehicle dynamics model was validated via steering wheel angle step input and serpentine and brake tests, and has a high confidence level, with the deviation of each metric being less than 10%. The influence regularities of the suspension damping ratio on ride comfort and handling stability were analyzed. In terms of ride comfort performance, the vehicle body acceleration (wheel dynamic load) RMS consistently increases (decreases) with increasing damping ratio, and the sensitivity of the RMS values of both vehicle body acceleration and wheel dynamic load to damping ratio variations becomes progressively more pronounced as road conditions deteriorate. In terms of handling stability performance, increasing suspension damping can effectively improve the transient response characteristics of both lateral and longitudinal motions. This enhancement reduces the load transfer caused by

roll or pitch during dynamic responses, thereby improving the handling and stability performance of the vehicle in both lateral and longitudinal directions. Based on this foundation, a hybrid control strategy was proposed which utilizes ADD-SH control logic for vertical control and trigger rule-based control logic for lateral and longitudinal control. The effectiveness of the control strategy was validated through ride comfort and handling stability subjective and objective tests. The results show that the proposed hybrid control strategy reduces vehicle body vibration acceleration and improves vehicle dynamic response during steering and acceleration/braking conditions. In conclusion, the advantages of the developed control strategy are obvious, and the strategy is intuitive and easy to apply in the actual vehicle development processes. However, the control effects are not optimal because the evaluation metrics of handling stability and ride comfort are not completely analyzed in an optimized process.

Author Contributions: F.W., conceptualization, methodology, original draft preparation, resources, and formal analysis; H.W., methodology, software, writing—review and editing, visualization, and formal analysis; S.X., investigation, data curation, supervision, project administration, and funding acquisition. All authors have read and agreed to the published version of the manuscript.

Funding: This research was funded by the Chengdu Technological University Fund Project, grant number 244265.

Data Availability Statement: Data is contained within the article.

Conflicts of Interest: The authors declare no conflicts of interest.

References

1. Rivera, S.; Kouro, S.; Vazquez, S.; Goetz, S.; Lizana, R.; Romero-Cadaval, E. Electric Vehicle Charging Infrastructure: From Grid to Battery. *IEEE Ind. Electron. Mag.* **2021**, *15*, 37–51. [CrossRef]
2. Yang, M.; Dai, P.; Yin, Y.; Wang, D.; Wang, Y.; Huang, H. Predicting and Optimizing Pure Electric Vehicle Road Noise via a Locality-Sensitive Hashing Transformer and Interval Analysis. *ISA Trans.* **2025**, *157*, 556–572. [CrossRef]
3. Huang, H.; Wang, Y.; Wu, J.; Ding, W.; Pang, J. Prediction and Optimization of Pure Electric Vehicle Tire/Road Structure-Borne Noise Based on Knowledge Graph and Multi-Task ResNet. *Expert Syst. Appl.* **2024**, *255*, 124536. [CrossRef]
4. Huang, H.; Li, R.; Yang, M.; Lim, T.; Ding, W. Evaluation of vehicle interior sound quality using a continuous restricted Boltzmann machine-based DBN. *Mech. Syst. Signal Process.* **2017**, *84*, 245–267. [CrossRef]
5. Zhou, S.; Walker, P.; Tian, Y.; Nguyen, C.T.; Zhang, N. Comparison on Energy Economy and Vibration Characteristics of Electric and Hydraulic in-Wheel Drive Vehicles. *Energies* **2021**, *14*, 2290. [CrossRef]
6. Medina, H.; Carpenter, N. Transverse Third-Damper to Improve Suspension Systems for In-Wheel Motor Driven Electric Vehicles. *J. Dyn. Syst. Meas. Control* **2023**, *145*, 031003. [CrossRef]
7. Zhao, J.; Yin, Y.; Chen, J.; Zhao, W. Evaluation and Prediction of Vibration Comfort in Engineering Machinery Cabs Using Random Forest with Genetic Algorithm. *SAE Int. J. Veh. Dyn. Stab. NVH* **2024**, *8*, 491–512. [CrossRef]
8. Zhu, H.; Zhao, J.; Wang, Y.; Ding, W.; Pang, J.; Huang, H. Improving of Pure Electric Vehicle Sound and Vibration Comfort Using a Multi-Task Learning with Task-Dependent Weighting Method. *Measurement* **2024**, *233*, 114752. [CrossRef]
9. Samaroo, K.; Awan, A.W.; Marimuthu, S.; Iqbal, M.N.; Daniel, K.; Shabbir, N. Performance Investigation of Active, Semi-Active and Passive Suspension Using Quarter Car Model. *Algorithms* **2025**, *18*, 100. [CrossRef]
10. Feng, J.; Liang, J.; Lu, Y. An Integrated Control Framework for Torque Vectoring and Active Suspension System. *Chin. J. Mech. Eng.* **2024**, *37*, 10. [CrossRef]
11. Yan, S.; Sun, W.; Gao, H. Vibration Suppression for Motor-Driven Uncertain Active Suspensions with Hard Constraints and Analysis of Energy Consumption. *IEEE Trans. Syst. Man Cybern. Syst.* **2022**, *52*, 618–630. [CrossRef]
12. Savaia, G.; Sohn, Y.; Formentin, S.; Panzani, G.; Corno, M.; Savaresi, S.M. Experimental Automatic Calibration of a Semi-Active Suspension Controller via Bayesian Optimization. *Control Eng. Pract.* **2021**, *112*, 104826. [CrossRef]
13. Chen, X.; Wang, Z.; Shi, H.; Jiang, N.; Zhao, S.; Qiu, Y.; Liu, Q. Review of Agricultural Machinery Seat Semi-Active Suspension Systems for Ride Comfort. *Machines* **2025**, *13*, 246. [CrossRef]
14. Alexandru, C. A Method for Finding the Static Equilibrium of the Non-Steered Wheel Suspension Systems Used in Passenger Cars. *Appl. Sci.* **2022**, *12*, 7122. [CrossRef]

15. Lee, G.; Hyun, M.; Kang, D. High-Efficiency Active Suspension Based on Continuous Damping Control. *Int. J. Automot. Technol.* **2022**, *23*, 31–40. [CrossRef]
16. Kaldas, M.; Rivas, J.; Soliman, A. Initial Pitch Control for Semi-Active Suspension System. *SAE Int. J. Veh. Dyn. Stab. NVH* **2022**, *6*, 405–419. [CrossRef]
17. Zhang, N.; Zhao, Q.; Huang, S. Optimal Sliding Mode Hierarchical Decoupled Control of Vehicle Semi-Active Suspension. *Veh. Syst. Dyn.* **2024**, 1–31. [CrossRef]
18. Han, K.; Hu, Y.; Zeng, D.; Yu, Y.; Xiao, L.; Yang, J.; Liu, W.; Gao, L. Vehicle Attitude Control of Magnetorheological Semi-Active Suspension Based on Multi-Objective Intelligent Optimization Algorithm. *Actuators* **2024**, *13*, 466. [CrossRef]
19. Čorić, M.; Deur, J.; Kasać, J.; Tseng, H.E.; Hrovat, D. Optimisation of Active Suspension Control Inputs for Improved Vehicle Handling Performance. *Veh. Syst. Dyn.* **2016**, *54*, 1574–1600. [CrossRef]
20. Lai, F.; Jiang, C.Y. Establishment and Simulation Analysis of 18 DOF Unified Dynamics Model of Automobile Chassis. *Int. J. Control Autom. Syst.* **2021**, *19*, 2323–2342. [CrossRef]
21. Ataei, M.; Khajepour, A.; Jeon, S. Development of a Novel General Reconfigurable Vehicle Dynamics Model. *Mech. Mach. Theory* **2021**, *156*, 104147. [CrossRef]
22. Kou, F.; Wang, R.; Hong, F.; Yang, H. Adaptive Backstepping Control of Semi-Active Suspension with Built-In Solenoid Valve. *J. Vib. Shock* **2022**, *41*, 1972–1992. [CrossRef]
23. Tudón-Martínez, J.C.; Lozoya-Santos, J.J.; Morales-Menendez, R.; Ramirez-Mendoza, R.A. An Experimental Artificial-Neural-Network-Based Modeling of Magneto-Rheological Fluid Dampers. *Smart Mater. Struct.* **2012**, *21*, 085007. [CrossRef]
24. Chen, J.; Yu, C.; Wang, Y.; Zhou, Z.; Liu, Z. Hybrid Modeling for Vehicle Lateral Dynamics via AGRU with a Dual-Attention Mechanism Under Limited Data. *Control Eng. Pract.* **2024**, *151*, 106015. [CrossRef]
25. Lee, G.H.; Kim, D.-H.; Pak, J.M.; Ahn, C.K. Vehicle Sideslip Angle Estimation Using Finite Memory Estimation and Dynamics/Kinematics Model Fusion Based on Neural Networks. *IEEE Trans. Intell. Transp. Syst.* **2025**, *26*, 2157–2168. [CrossRef]
26. Wen, H.; Huang, H.; Zhang, W. Research of Time Lag Characteristics of Pilot-Operated Solenoid Valve Damper Based on Multi-Physics Field. *Proc. Inst. Mech. Eng. Part D J. Automob. Eng.* **2025**, *239*, 1660–1684. [CrossRef]
27. Hemanth, K.; Kumar, H.; Gangadharan, K.V. Vertical Dynamic Analysis of a Quarter Car Suspension System with MR Damper. *J. Braz. Soc. Mech. Sci. Eng.* **2017**, *39*, 41–51. [CrossRef]
28. Mata, G.T.; Kumar, H.; Mahalingam, A. Performance Analysis of a Semi-Active Suspension System Using Coupled CFD-FEA Based Non-Parametric Modeling of Low Capacity Shear Mode Monotube MR Damper. *Proc. Inst. Mech. Eng. Part D J. Automob. Eng.* **2018**, *233*, 1214–1231. [CrossRef]
29. Yoon, D.-S.; Choi, S.-B. Adaptive Control for Suspension System of In-Wheel Motor Vehicle with Magnetorheological Damper. *Machines* **2024**, *12*, 433. [CrossRef]
30. Zhang, H.; Qi, Y.; Si, W.; Zhang, C. An Improved Adaptive Sliding Mode Control Approach for Anti-Slip Regulation of Electric Vehicles Based on Optimal Slip Ratio. *Machines* **2024**, *12*, 769. [CrossRef]
31. Zhang, K.; As'arry, A.; Zhu, L.; Hairuddin, A.A.; Hassan, M.K.; Zain, M.Z.M. Enhancing Ride Comfort of Semi-Active Suspension Through Collaboration Control Using Dung Beetle Optimizer Optimized Fuzzy PID Controller. *Adv. Mech. Eng.* **2025**, *17*, 1–14. [CrossRef]
32. Li, G.; Huang, Q.; Ni, L.; Zhou, X.; Zhou, C.; Hu, G. Research on Compound Control Strategy of Vehicle Magnetorheological Semi-Active Suspension. *Mod. Manuf. Eng.* **2022**, *8*, 1–9. [CrossRef]
33. Liang, J.; Lu, Y.; Pi, D.; Yin, G.; Zhuang, W.; Wang, F. A Decentralized Cooperative Control Framework for Active Steering and Active Suspension: Multi-Agent Approach. *IEEE Trans. Transp. Electrif.* **2022**, *8*, 1414–1429. [CrossRef]
34. Kim, J.; Lee, T.; Kim, C.-J.; Yi, K. Model Predictive Control of a Semi-Active Suspension with a Shift Delay Compensation Using Preview Road Information. *Control Eng. Pract.* **2023**, *137*, 105584. [CrossRef]
35. Piñón, A.; Favela-Contreras, A.; Félix-Herrán, L.C.; Beltran-Carbajal, F.; Lozoya, C. An ARX Model-Based Predictive Control of a Semi-Active Vehicle Suspension to Improve Passenger Comfort and Road-Holding. *Actuators* **2021**, *10*, 47. [CrossRef]
36. Savaia, G.; Formentin, S.; Panzani, G.; Corno, M.; Savaresi, S.M. Enhancing Skyhook for Semi-Active Suspension Control via Machine Learning. *IFAC J. Syst. Control* **2021**, *17*, 100161. [CrossRef]
37. Lee, D.; Jin, S.; Lee, C. Deep Reinforcement Learning of Semi-Active Suspension Controller for Vehicle Ride Comfort. *IEEE Trans. Veh. Technol.* **2023**, *72*, 327–339. [CrossRef]
38. Qin, Y.; Dong, M.; Zhao, F.; Gu, L. Suspension Semi-Active Control of Vehicles Based on Road Profile Classification. *J. Northeast. Univ. (Nat. Sci.)* **2016**, *37*, 1138–1143.
39. Michelberger, P.; Palkovics, L.; Bokor, J. Robust Design of Active Suspension System. *Int. J. Veh. Des.* **1993**, *14*, 145–165. [CrossRef]
40. Wu, Z.C.; Chen, S.Z.; Yang, L.; Zhang, B. Model of Road Roughness in Time Domain Based on Rational Function. *Trans. Beijing Inst. Technol.* **2009**, *29*, 795–798.
41. Ren, H.; Chen, S.; Zhao, Y.; Liu, G.; Yang, L. State observer-based sliding mode control for semi-active hydro-pneumatic suspension. *Veh. Syst. Dyn.* **2016**, *54*, 168–190. [CrossRef]

42. Shi, P.; Zhao, Q.; Wang, K.; Zhang, R.; Xiao, P. Simulation and Verification Analysis of the Ride Comfort of an In-Wheel Motor-Driven Electric Vehicle Based on a Combination of ADAMS and MATLAB. *Int. J. Model. Simul. Sci. Comput.* **2022**, *13*, 2250002. [CrossRef]
43. Niu, Z.; Xin, S.; Liu, F. Design Method of Rack-and-Pinion Pair with Pure Rolling Variable Transmission Ratio. *Proc. Inst. Mech. Eng. Part C J. Mech. Eng. Sci.* **2024**, *238*, 7354–7372. [CrossRef]
44. Yun, S.; Lee, J.; Jang, W.; Kim, D.; Choi, M.; Chung, J. Dynamic Modeling and Analysis of a Driving Passenger Vehicle. *Appl. Sci.* **2023**, *13*, 5903. [CrossRef]
45. Hu, T.; Jiang, L.; Pan, L.; Chen, B.; Gong, N.; Yang, J.; Gong, X.; Sun, S. Development of a Semi-Active Suspension Using a Compact Magnetorheological Damper with Negative-Stiffness Components. *Mech. Syst. Signal Process.* **2025**, *223*, 111842. [CrossRef]
46. *GB/T 6323-2014*; Controllability and stability test procedure for automotive. Standardization Administration of the People's Republic of China: Beijing, China, 2014.
47. Xu, X.; Su, P.; Wang, F. Coordinated Control of Dual-Motor Using the Interval Type-2 Fuzzy Logic in Autonomous Steering System of AGV. *Int. J. Fuzzy Syst.* **2021**, *23*, 1070–1086. [CrossRef]
48. An, Y.; Wang, L.; Deng, X.; Chen, H.; Lu, Z.; Wang, T. Research on Differential Steering Dynamics Control of Four-Wheel Independent Drive Electric Tractor. *Agriculture* **2023**, *13*, 1758. [CrossRef]
49. Cheng, Y.; Hu, R.; Xu, W.; Yu, L. Integrated Control Strategy of Semi-Active Suspension and In-Wheel Motors for Handling Limit of Electric Race Car. *Proc. Inst. Mech. Eng. Part D J. Automob. Eng.* **2023**, *238*, 4486–4504. [CrossRef]
50. Zhao, L.; Zhou, C.; Yu, Y. A Research on Optimal Damping Ratio Control Strategy for Semi-Active Suspension System. *Automot. Eng.* **2018**, *40*, 41–47. [CrossRef]
51. Huang, H.; Lim, T.C.; Wu, J.; Ding, W.; Pang, J. Multitarget Prediction and Optimization of Pure Electric Vehicle Tire/Road Airborne Noise Sound Quality Based on a Knowledge- and Data-Driven Method. *Mech. Syst. Signal Process.* **2023**, *197*, 110361. [CrossRef]
52. Huang, H.; Huang, X.; Ding, W.; Yang, M.; Yu, X.; Pang, J. Vehicle Vibro-Acoustical Comfort Optimization Using a Multi-Objective Interval Analysis Method. *Expert Syst. Appl.* **2023**, *213*, 119001. [CrossRef]
53. Negash, B.A.; You, W.; Lee, J.; Lee, C.; Lee, K. Semi-Active Control of a Nonlinear Quarter-Car Model of Hyperloop Capsule Vehicle with Skyhook and Mixed Skyhook-Acceleration Driven Damper Controller. *Adv. Mech. Eng.* **2021**, *13*, 1–14. [CrossRef]
54. *GB/T 4970-2009*; Method of Running Test–Automotive Ride Comfort. Standardization Administration of the People's Republic of China: Beijing, China, 2009.
55. *ISO 2631-1:1997*; Mechanical Vibration and Shock–Evaluation of Human Exposure to Whole-Body Vibration–Part 1: General Requirements. International Organization for Standardization: Geneva, Switzerland, 1997.
56. Yin, C.; Luo, D.; Yue, S. Study on Vibration Performance of Commercial Vehicle's Cab-Seat Mounting System. *J. Mach. Des.* **2023**, *40*, 99–107. [CrossRef]
57. Zhuang, C.; Wen, H.; Ni, X.; Zhang, D.; Bao, Y.; Huang, H. Optimization of Cab Vibration Comfort for Construction Machinery Based on Multi-Target Regression Forests. *Machines* **2022**, *10*, 1148. [CrossRef]
58. Chen, S.; Zhao, Z.; Zhao, K. Coordinated Control of Trajectory Tracking and Yaw Stability of Four-Wheel-Independent-Drive Autonomous Electric Vehicles. *J. Tongji Univ. (Nat. Sci.)* **2024**, *52*, 185–196.
59. *ISO 3888-1:2018*; Passenger Cars–Test Track for a Severe Lane-Change Manoeuvre–Part 1: Double Lane-Change. International Organization for Standardization: Geneva, Switzerland, 2018.
60. Huang, H.; Huang, X.; Ding, W.; Zhang, S.; Pang, J. Optimization of Electric Vehicle Sound Package Based on LSTM with an Adaptive Learning Rate Forest and Multiple-Level Multiple-Objective Method. *Mech. Syst. Signal Process.* **2023**, *187*, 109932. [CrossRef]

Disclaimer/Publisher's Note: The statements, opinions and data contained in all publications are solely those of the individual author(s) and contributor(s) and not of MDPI and/or the editor(s). MDPI and/or the editor(s) disclaim responsibility for any injury to people or property resulting from any ideas, methods, instructions or products referred to in the content.